Development of a near-infrared optical feedback cavity enhanced absorption spectometer (OF-CEAS) for atmospheric water vapor isotope ratio (18 O/16 O, 17 O/16 O, and 2 H/1 H) measurements

Iannone, Rosario

Chapter 2

Methods of Stable Isotope Ratio Measurements on Water

2.1 Isotope Ratio Mass Spectrometry

Mass spectrometry is the main technique used to measure isotope abundances. It is based on the motion of charged particles through an electric and magnetic field, measuring the mass to charge ratio of ions. The underlying components of a gas source isotope ratio mass spectrometer are an inlet system, an ion source, a flight tube, an ion collector assembly, and finally a recording system.

The classical configuration for isotope analysis is a dual-inlet system, in which the sample and the reference are measured relative to one another. The gas enters a source region, where it is ionized and then focused into a coherent beam by several electric lenses. The resulting beam passes through a strong magnetic field, which forces the ions into a circular trajectory. Light ions are deflected more strongly than heavy ions with the same charge and, after acceleration to the same kinetic energy, this results in a spatial separation of ions of different isotopologues of the molecules to analyze. The ions impinge on several collectors, called Faradays cups. The intensity of these ion beams is proportional to the isotopologue abundance.

Isotope Ratio Mass Spectrometer (IRMS) allows precise measurements of stable isotope ratios. The IRMS instrument was designed by Nier in 1937, and over the last 40 years it has much benefited of continued research and development.

One of the peculiarities of isotope ratio mass spectrometry is that most samples must be pre-processed off-line to produce gases that can be introduced into the ion source. Water vapor for instance is not compatible with the vacuum system of the IRMS and requires chemical conversion (e.g., to CO_2 or H_2) prior to introduction into the spectrometer.

To concentrate on water isotopes, the measurement of $\delta^{18}O$ in water is conventionally obtained by equilibration with CO_2 [Epstein and Mayada, 1953]. During this equilibration, the oxygen atoms belonging to the water and carbon dioxide exchange through the bicarbonate reaction. If the molar amount of CO_2 is much smaller than that of water, after equilibration the $\delta^{18}O$ of water has been transferred to that of CO_2. However, the $\delta^{18}O$ of CO_2 and H_2O retain a significant, temperature-dependent difference, characteristic for the exchange process. Careful operation of the process (that is, constant and fixed temperature, constant amounts of water and CO_2, etc.) makes a precision of these measurements of 0.05‰ or better possible.

Alternatively, electrolysis of water decomposes H_2O into O_2 and H_2 in gaseous phase due to an electric current that passes through the water. Meijer and Li [1998] used electrolysis with $CuSO_4$ as electrolyte, transforming water into H_2SO_4, and oxygen gas, which was afterwards analyzed with an isotope ratio mass spectrometer. They obtained an accuracy of 0.10‰ for $\delta^{18}O$, and 0.07‰ for $\delta^{17}O$. The ability to measure $\delta^{17}O$ is rather unique to this method.

For the δ^2H measurement of water, the classical procedure is the reduction of water to hydrogen gas at 800°C with the aid of uranium [Bigeleisen et al., 1952], or with zinc at 500 °C [Friedman, 1953]. Because of the fractionation effects accompanying the reduction reaction, a complete reduction of the water sample is crucial. The typical precision of this method is 1‰. An alternative method is the equilibration of water and H_2 in the presence of a platinum catalyst. But this method is accompanied by a very large isotope fractionation, of about -740‰ at room temperature, that is also highly temperature dependent [Horita and Gat 1988; Coplen et al., 1991].
These sample pre-treatments are time consuming (and sometimes hazardous, as for the reduction over hot uranium) and they represented a limiting factor in achieving the high accuracy required in the majority of studies. Furthermore the amount of water required is typically 1 ml or more, making the use of the off-line sample pre-treatment impossible for many atmospheric applications. For small samples (< 0.1 ml) the chemical conversion of water becomes more complicated and vulnerable. Many details of the conversions become more important, such as, for example, that the isotopic equilibration with CO_2 performed for $\delta^{18}O$ measurements, as described above, involves a considerable change in the isotopic composition of the water sample [Horita, 1988] that needs to be corrected for, whereas the conversion of microliters of water to H_2, by means of uranium produces a big memory effect [Begley and Scrimgeour, 1997].

The invention of so-called continuous-flow isotope ratio mass spectrometry (CF-IRMS) represented a real step up in the field of mass spectrometry. The crucial idea was that IRMS also functions when the sample is not introduced purely into a high vacuum inlet system, but rather carried by a flow of Helium. By doing so, a whole range of long-developed, automatic and compact chemical pre-treatment systems

became available to IRMS. These were e.g. elemental analyzers, gas chromatographic separation, pyrolysis, and reduction systems. All of these deal with small samples and automatic sample introduction, such that the whole preparation system could be combined with the IRMS into one automated system.

Starting in the 1990's, CF-IRMS developed rapidly, delivering fast, on-line sample conversion. CF-IRMS is capable of analyzing much smaller sample but offers lower precision compared to the traditional dual-inlet system [Sharp, 2007]. Especially the isotope measurements of water profited very much from these developments. Morrison et al. [2001] described an automatic, on-line method for the δ^2H measurements of small water samples using reduction on hot chromium, and they reported a precision of 0.5‰ on water sample of 0.5 µl.

Alternatively, on-line pyrolysis, producing H_2 and CO, enables the combined measurement of δ^2H and $\delta^{18}O$ [Begeley and Scrimcour, 1997].

Modern commercial mass spectrometer systems are now completely automated for this analysis. The hot furnace and the liquid autosampler are fully integrated. A syringe automatically injects a few microliters of water sample into a heated injection room, where the water goes from the liquid into the vapor phase. The sample then follows a He flow and is introduced into the hot furnace at 1450 °C where the reaction takes place. Both H_2 and CO are produced, and subsequently separated in time by a GC column. Then the sample enters the mass spectrometer, which starts analyzing masses 2 and 3 (HH/HD), and switches after a specified time interval to masses 28, 29 and 30 (CO molecules containing ^{16}O, ^{13}C, and ^{18}O, respectively). The precision for this IRMS spectrometer is at best 0.5‰ and 0.1‰ for δ^2H and $\delta^{18}O$, respectively, requiring 0.2 µl of water.

As seen above, IRMS can deliver a very high level of precision for isotope ratio measurements. Still, IRMS instruments are rather complicated instruments with a high vacuum system, and are not very suitable for in-situ applications.

Another, principal limitation is the difficulty to distinguish between different, but same-mass isotopologues. This is for example the case for $^{17}O/^{16}O$-analyses on water using the CO_2-equilibration or pyrolysis methods, since the ^{17}OCO and $^{13}CO_2$, or $C^{17}O$ and ^{13}CO, molecules are detected in the same mass channel.

The previously mentioned electrolysis preparation solves this problem, as does any other conversion of water into molecular oxygen gas, e.g. by cobalt fluoride [Baker et al., 2002].

Whereas IRMS represents the most widespread methodology for the determination of isotope ratios, nevertheless alternative techniques have been developed and used to measure isotope ratios. Nuclear Magnetic Resonance (NMR) spectroscopy is well-suited to δ^2H-measurements on a number of species. The technique has been mainly used in the field of food authenticity [Martin and Martin, 1995]. The precision of this technique is not high enough for environmental applications. Furthermore, this technique is complicated, and perhaps even less suited for in situ measurements than IRMS. An overview of the basic principle of ^{2}H-NMR spectroscopy is given by Rezzi et al., [2004].

So far, only optical methods are able to measure both the oxygen and hydrogen isotopic composition of water in combined measurements and without any kind of pre-treatments. Kerstel et al. [1999] reported the first simultaneous determination of δ^2H, δ^{17}O and δ^{18}O by means of infrared laser spectroscopy with a precision of 0.7‰ for δ^2H and 0.5 ‰ for δ^{17}O and δ^{18}O, using 10 µl water samples.

2.2 Optical Methods

Optical systems, based on laser spectroscopy, were introduced as an alternative to IRMS, with potentially many advantages. The infrared region is often referred to as the “finger-print” region of the optical spectrum where many molecules show rotation-vibration absorption bands. At sufficiently low pressure, these spectra consist of a number of discrete absorption lines, which have a certain line-width and shape that depend on temperature and pressure. Different infrared detection techniques have been developed to satisfy the requirements for more sensitive and precise and faster analyses in industrial and monitoring applications. We cite among these techniques Photoacoustic Spectroscopy (PAS) [Matsume et al., 1998], Opto Galvanic Spectroscopy [Murnick et al., 1998], Non Dispersive Infrared Spectroscopy (NDIR), Fourier Transform Infrared Spectroscopy (FTIR) [Fusch et al., 1993; Griffith et al. 2006], and Tunable Diode Laser Absorption Spectroscopy (TDLAS) [Werle, 1998;

Curl and Tittel, 2002], as well as a number of cavity enhanced techniques [Berden et al., 2000; Mazurenka et. al., 2005].

Infrared laser absorption spectroscopic detection techniques in particular, are highly quantitative and are sufficiently sensitive and precise to enable isotope ratio determinations. The next paragraphs describe the theory and applications of infrared laser absorption measurements and will introduce many concepts, relevant for the understanding of the following chapters.

2.2.1 Interaction of Electromagnetic Radiation with Molecules

Gas phase direct absorption laser spectroscopy is described by the Lambert-Beer Law. Consider radiation with intensity I_0, passing through an absorption cell of length l, filled with absorbing medium with a concentration c. Let I be the intensity of the radiation coming out from the cell. The Lambert-Beer Law asserts that the attenuation of the intensity of the radiation through an absorbing species is decreasing exponentially with l:

$$I = I_0 \exp(-\alpha(\nu)l) \tag{2.1}$$

Where ν is the frequency of the radiation. The exponent $\alpha(\nu)\cdot l$ is known as the optical thickness of the medium, while $\alpha(\nu)$ is the absorption coefficient. The dimension of I and I_0 is energy per unit area. It is important to notice that the Lambert-Beer Law is valid in the linear absorption regime. The absorption coefficient $\alpha(\nu)$ can be written as follows:

$$\alpha(\nu) = \sigma(\nu)n \tag{2.2}$$

Where n represents the molecular number density. $\sigma(\nu)$ is known as the cross section. The cross section depends on the frequency ν through a function called line profile g (ν-ν_0). In particular:

$$\sigma = Sg(\nu - \nu_0) \tag{2.3}$$

Thus:

$$\alpha(\nu)\cdot l = S\cdot g(\nu-\nu_0)\cdot n\cdot l \tag{2.4}$$

The function $g(\nu\text{-}\nu_0)$ depends on pressure and temperature, and it is normalized such that:

$$\int_{-\infty}^{+\infty} g(\nu)d\nu = 1 \tag{2.5}$$

S is the linestrength of the absorption transition and it is a fundamental spectroscopic property of the absorbing species. Particularly, *S* arises from Boltzmann statistics governing the distribution of population among the available internal energy levels. *S*, therefore, depends on the number of molecules in the lower level of the transition (see paragraph 2.2.2), and it is in general temperature-dependent. A change in temperature will redistribute the population over the rotational levels of the ground vibrational state. For a given transition from an initial state to a final state *S* depends on the temperature *T*, according the following equation [see, e.g., Measures, M. R., 1997]:

$$S(T) = S(T_0)\frac{Q(T_0)}{Q(T)}\left(\frac{T_0}{T}\right)\exp\left[-hc\frac{E''}{k}\left(\frac{1}{T}-\frac{1}{T_0}\right)\right]\left[-\exp\left(\frac{-hc\nu_0}{kT}\right)\right]\left[1-\exp\left(\frac{-hc\nu_0}{kT_0}\right)\right]^{-1} \tag{2.6}$$

S (T_0) is the line strength at reference temperature T_0 and *E"* is lowest energetic level of the transition, with *h*, *c* and *k* being the Planck constant, the speed of light (in vacuum) and the Boltzmann constant, respectively. *Q* (*T*) represents the ro-vibrational partition function of the molecule and it can be approximated by using a second order polynomial such as: $a+bT+cT^2+dT^3$.

The linestrength *S* can be expressed in a large number of units, depending on the way the absorption coefficient is defined. Frequently used units to express the above parameters are:

l: cm;

n: molecules/cm^3;

σ: cm^2/molecule;

g: $\frac{1}{\text{cm}^{-1}} = \text{cm}$;

S: $\frac{1}{\text{cm}} \cdot \frac{\text{cm}^3}{\text{molecule}} \cdot \frac{1}{\text{cm}} = \text{cm}/\text{molecule}$.

Absorption does not only occur at a single frequency but has a frequency distribution around the line center. The shape of the absorption profile has a theoretical minimal value (often called the natural line shape and width), which is connected to the lifetime of the excited species. In most cases, the profile is, however, broadened by a number of mechanisms. If the lineshape originates from a homogeneously (natural lifetime or collision) broadened transition, it is represented by a Lorentzian function, whereas in case of inhomogeneously (Doppler) broadened media, the line shape is a Gaussian function.

A spectral line whose distribution is Lorentzian is expressed by the following equation [see, e.g., Measures, M. R., 1997]:

$$g(\nu - \nu_0) = \frac{\left(\gamma/\pi\right)}{\left[(\nu - \nu_0)^2 + \gamma^2\right]} \tag{2.7}$$

where γ is the Half Width at Half Maximum (HWHM) of the line.

Generally, the natural linewidth of an atomic or molecular transition cannot be observed without very sophisticated spectroscopic techniques, because of the presence of other broadening effects. In practice, at low pressure and ambient temperature, gas phase molecular absorptions are broadened because of the Doppler effect, resulting from thermal motions, and because of interactions between molecules (collisional or pressure broadening). In fact, when collisions occur between molecules there is also the possibility of energy exchange, which leads effectively to a speed-dependent broadening of the line.

However, in many cases, Doppler broadening and collisional broadening can be treated as independent phenomena.

The normalized Doppler absorption shape function can be written as [see, e.g., Measures, 1997]:

$$g(\nu-\nu_0)=\left(1/\Gamma_D\right)\left(\ln 2/\pi\right)^{1/2}\exp\left[-(\nu-\nu_0)^2\ln 2/\Gamma_D^2\right] \tag{2.8}$$

The HWHM of the line profile is:

$$\Gamma_D=\frac{\nu_0}{c}\left(2\ln 2\cdot\frac{kT}{M}\right)^{1/2} \tag{2.9}$$

Where c is the light speed, k is the Boltzmann constant, T is the temperature, and M the atomic mass.

Also, collisional broadening needs to be taken into account. During the interaction among neighboring atoms or molecules, the energy states are perturbed producing an additional line broadening [see, e.g., Hollas, 1992]:

$$\Delta\nu=(2\pi\tau)^{-1} \tag{2.10}$$

Here τ is the mean time between collisions. This line broadening is homogeneous and produces a Lorentzian line shape.

The collisional and Doppler broadening effects coexist. Thus, for an exact interpretation of experimental results it is necessary to combine the Lorentzian and Doppler width. In many cases, the profile of the spectral line can then be approximated by a Voigt function. This function is the result of the convolution of the Doppler function with a Lorentzian function [see, e.g., Whiting, 1968]:

$$V(x) = L \otimes G \tag{2.11}$$

The Voigt lineshape may also be defined in the following manner [see, e.g., Humlicek, 1982]:

$$V(x) = C\frac{y}{\pi}\int_{-\infty}^{+\infty}\frac{e^{-t^2}}{y^2 + (x-t)^2}dt \qquad (2.12)$$

Where *V(x)* is an area- normalized function,

$$C = \frac{\sqrt{\ln 2}}{\Delta\Gamma_D\sqrt{\pi}}\ ,\quad y = \sqrt{\ln 2}\frac{\Delta\gamma_L}{\Delta\Gamma_D}$$

and

$$x = \frac{(\nu - \nu_0)\sqrt{\ln 2}}{\Delta\Gamma_D}$$

Where ν_0 is the line center position, $\Delta\gamma_L$ the collisional HWHM and $\Delta\Gamma_D$ the calculated Doppler HWHM. The physical significance of the convolution is that asymptotically, for large pressure the Voigt profile approaches the Lorentzian profile, while at low pressure the Voigt profile approaches the Gaussian one. For intermediate situations, in practice a pressure range between typically 5 and 100 Torr, calculation of the Voigt profile is necessary to obtain numerically accurate information about the spectra.

The Voigt profile is still only an approximation, since it does not take into account the effect of velocity-changing collisions, which is responsible for the random motion of the active molecules.

A deviation of the Voigt profile can occur because of a significant narrowing of the Doppler component. This effect is generally referred to as Dicke narrowing, and it is attributed to frequent velocity-changing collisions.

Two different physical models have been used to derive the narrowed spectral line shape profile. If we name with m_1 the molecular mass of the infrared active molecule and with m_2 the molecular mass of the perturber, than we distinguish [Lepère et al., 2001]:

1. Rautian model: where $m_1 << m_2$
2. Galatry model: where $m_1 >> m_2$.

This effect is characterized by a narrowing parameter β^0. The mathematical approach for the Rautian and Galatry profiles is illustrated in Lepère [2004]. From laboratory spectroscopic experiments, it has been shown that these two line models give better agreement between the experimental profile and the fitted profile. The residual observed, by the fitting procedure are notably reduced with the use of those two models compared to the Voigt one, indicating that the Dicke narrowing effect is not negligible, generally below 120 mbar (see Chapter 3 for an example).

2.2.2 Isotope Ratio Determination by Means of Laser Spectroscopy

Laser Absorption Spectroscopy is able to discriminate among the isotopologues of a molecule using the frequency shift of rotational-vibrational transitions observed in a molecular spectrum of gases when one atom is substituted by a different isotope.

In the classical picture, the nuclei of a molecule can vibrate around their internuclear axis. When two nuclei are different, as in the case of H_2O, the vibration causes a change in the electric moment of the molecule, which will show itself spectroscopically in vibrational bands. If the molecule has a permanent dipole moment, interaction with radiation can induce a transition from one vibrational state to another. At the same time, a molecule can also rotate around a perpendicular line to its inter nuclear axis. The rotational quantum is smaller than the vibrational one, and thus every change in the vibration will be characterized by a number of changes in the rotation. Water is an asymmetric molecule with the oxygen atom in the middle, characterized by three fundamental vibrational bands and strong rotational bands. The $H^{18}O$ H and the $H^{17}OH$ have vibrational and rotational frequencies slightly different from those of $H^{16}OH$, while $H^{16}O^2H$ has vibrational frequencies markedly different from those of the other isotopic forms. Figure 2.1 illustrates the general spectra for the isotopologues of the molecule of H_2O. Figure 2.1 was created using the HITRAN (High Resolution TRANsmission) database [Rothman et al., 2005], where molecular parameters such as line intensity and broadening coefficient, are collected.

Consider a simple spectroscopic experiment, where the laser beam enters a cell containing the absorbing species. By using laser absorption spectroscopy, two spectral lines, of which one belongs to the most abundant isotopic species *a* and the other to the less abundant species *x*, can be observed in the region scanned by the laser (Figure 2.2).

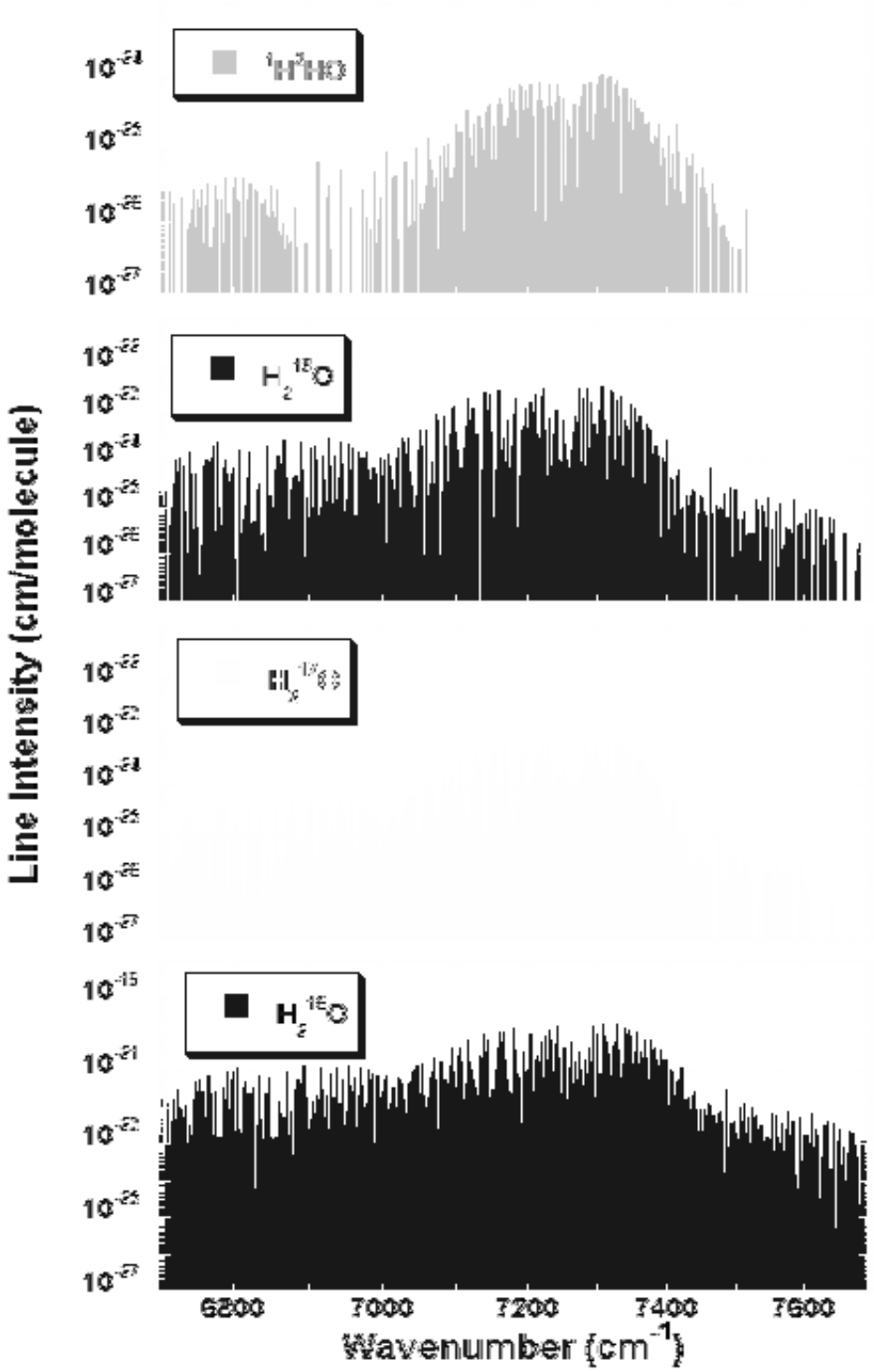

Figure 2.1: Overview of part of the $H_2{}^{16}O$, $H_2{}^{17}O$, $H_2{}^{18}O$, $^1H^{16}O^2H$ vibro-rotational spectra between 6700 and 7700 cm^{-1}, as calculated by HITRAN database. The line intensities correspond to their natural abundances in normal water.

The two lines find themselves in the same broadening conditions, namely the same temperature and pressure.

We can, either sequentially in the same cell, or at the same time in two cells, acquire two spectra corresponding to the sample gas and the reference gas, respectively.

The δ-value can be obtained from the "super ratio" of the absorption coefficient $\alpha(\nu_0)$ in the two spectra [Kerstel, 2004]:

$$\delta(x) = \frac{\left(\alpha_x(\nu_0)^{\text{sample}}/\alpha_x(\nu_0)^{\text{reference}}\right)}{\alpha_a(\nu_0)^{\text{sample}}/\alpha_a(\nu_0)^{\text{reference}}} - 1 = \frac{(\alpha_x(\nu_0)/\alpha_a(\nu_0))^{\text{sample}}}{(\alpha_x(\nu_0)/\alpha_a(\nu_0))^{\text{reference}}} - 1 \qquad (2.13)$$

Using (2.4), we thus find:

$$\delta(x) = \left(\frac{S_x^s/S_a^s}{S_x^r/S_a^r}\right)\left(\frac{g_x^s(0)/g_a^s(0)}{g_x^r(0)/g_a^r(0)}\right)\left(\frac{n_x^s/n_a^s}{n_x^r/n_a^r}\right)\left(\frac{l_x^s/l_a^s}{l_x^r/l_a^r}\right) - 1 \qquad (2.14)$$

Provided we keep the circumstances (pressure, temperature and path length) for reference and sample the same, all factors in (2.14) except the desired number density ratio, become unity. If the circumstances in the reference and sample cell would be different, the term containing the path length would still be =1, but due to different line widths, this would no longer be exactly true for the terms involving *S* and *g*. If, however, the temperature and pressure in the two cells are very similar, these terms become unity to a very good approximation.

Then, the only term remaining is:

$$\delta(x) = \left(\frac{n_x^s/n_a^s}{n_x^r/n_a^r}\right) - 1 \qquad (2.15)$$

Provided that the reference water is known on the international VSMOW-SLAP scale, the δ-value of the sample can thus be determined in this way.

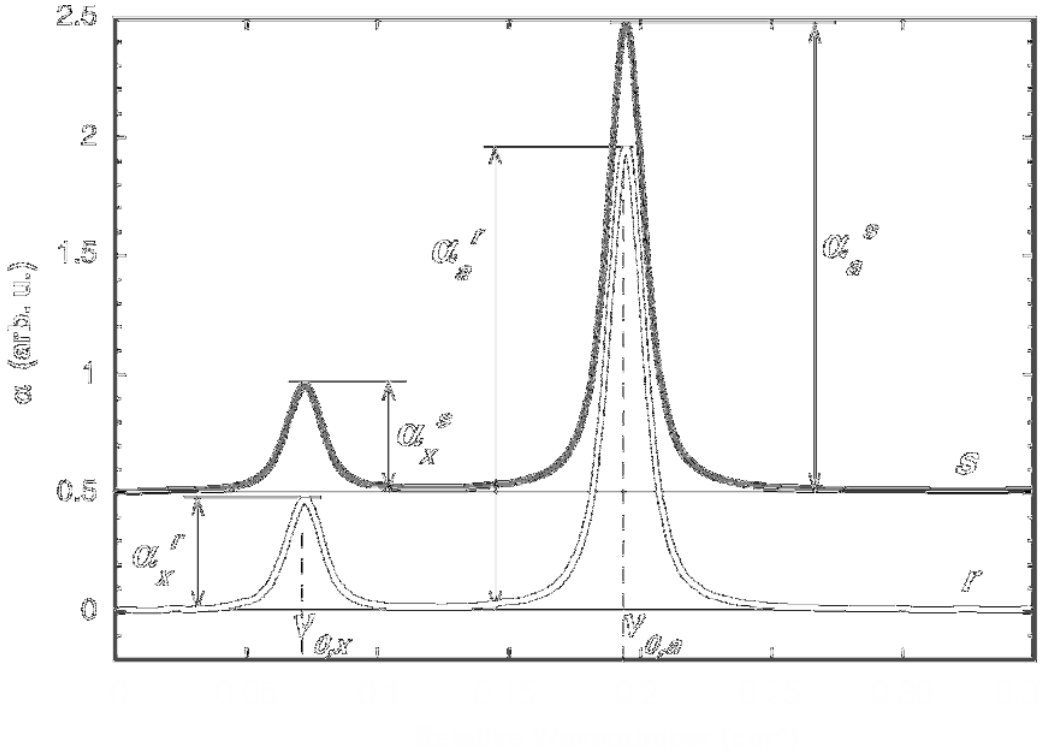

Figure 2.2: Infrared spectrum showing two rotational-vibrational transitions, both in the sample s and in the reference r. The weakest transition represents the less abundant specie while the strongest belongs to the most abundant one [From Kerstel, 2004].

2.3 Cavity Ring Down Spectroscopy (CRDS)

Cavity Ring Down Spectroscopy (CRDS) is a laser absorption spectroscopy method developed for the first time for measuring the reflectance of mirror coating [Herbelin et al., 1980; Anderson et al., 1984]. Afterwards, O'Keefe and Deacon [1988] realized that CRDS is applicable for measurements of the absorption spectrum of low absorption compounds. Thanks to the big progress in laser technology, CRDS is being used widely to detect atmospheric traces gases. The CRDS method is based on the determination of a time constant of the exponential decay of the laser light leaking out of a resonator or optical cavity. This represents the main difference of this technique compared to the conventional long path absorption spectroscopy where the determination of an absorption coefficient is related to the measurement of an intensity ratio.

2.3.1 Traditional Pulsed CRDS

The basic principle of CRDS is depicted in Figure 2.3.

In a typical cavity ring down experiment, a light pulse, with intensity I_0, is injected into an optical cavity composed by two highly reflective mirrors (R > 99.9%). The two mirrors are identical and they are characterized by curvature radii, R_1 and R_2 ($R_1 = R_2$), which vary between -25 cm and -100 cm. The distance l between the mirrors must be < 2R, such that the cavity forms a stable optical resonator. For the cavity to be stable, the radiation should be able to reproduce itself at any plane, while bouncing back and forth between the two mirrors. To achieve this condition it is necessary that [see, e.g., Siegman, 1986]:

$$0 \le \left(1 - \frac{l}{R_1}\right)\left(1 - \frac{l}{R_2}\right) \le 1 \qquad (2.16)$$

At the same time, the cavity is built as a cell, containing the absorbing medium. Any mirror is characterized by its field amplitude reflection coefficient r and its transmission coefficient t.

Normally these are complex-valued quantities. In general, the intensity reflectivity $R=|r|^2$ and transmittivity $T=|t|^2$ are the important values. No mirror is perfect: the mirror material absorbs or scatters some amount of the incident light. Either way, the light is lost. We can lump the energy loss in a single coefficient L. Energy conservation implies that the sum of light intensity reflection, transmission and loss is unity:

$$R + T + L = 1 \qquad (2.17)$$

The light travels back and forth between the mirrors. Usually the light pulse is shorter then the round trip in the cavity. This avoids spatial destructive interferences of the light pulse fraction in the cavity. Light intensity is transmitted out of the mirrors at each reflection and can be measured by a photodetector.

The output pulse has an exponential development:

$$I_{ringdown} = I_0 e^{-\frac{t}{\tau}} \tag{2.18}$$

The reciprocal of τ is also known as the ring-down rate.

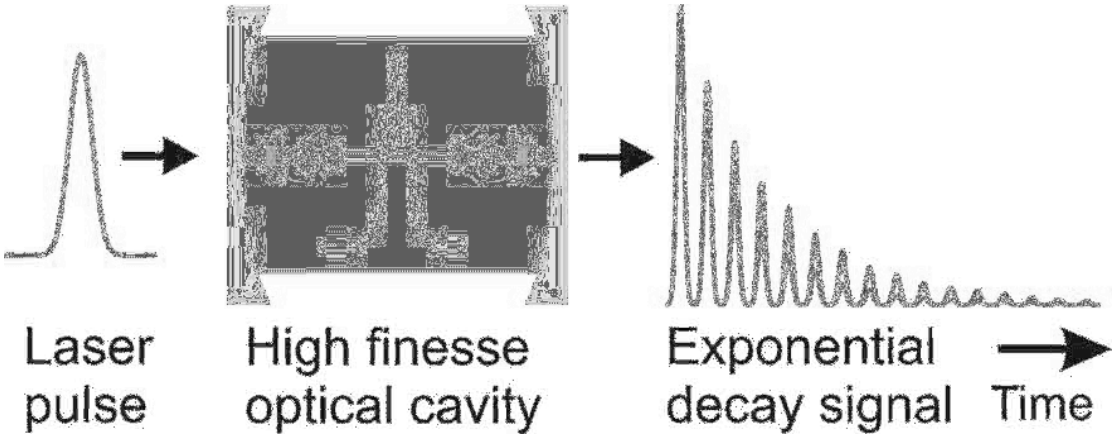

Figure 2.3: Ping-pong model of pulsed cavity ring down spectroscopy [from Paldus and Zare, 1999].

The ring down time τ does not depend on the amplitude of the light pulse and therefore it is not affected by intensity fluctuations. After the first passage through the cavity, the laser pulse initial intensity I_{in} will be attenuated to:

$$I_0 = T^2 e^{-\alpha l} I_{in} \tag{2.19}$$

Where α is the absorption coefficient of the absorbing medium, which fills the complete cavity. After a round trip inside the resonator the intensity is attenuated by a factor of $R^2 e^{-2\alpha l}$.

After *n* round trips the pulse intensity measured by a photodetector will have the following expression:

$$I_{ringdown} = \left[R e^{-\alpha l}\right]^{2n} I_0 = I_0 e^{-2n(-\ln R + \alpha l)} \tag{2.20}$$

We can transform the discrete number of passes *n* into a continuous time by introducing the time variable $t = 2 \cdot l \cdot n / c$ which represent the time that the light pulse spent inside the resonator.
Thus the Eq. (2.20) can be written as:

$$I_{ringdown} = I_0 e^{\frac{ct}{l}(-\ln R + \alpha l)} \tag{2.21}$$

The decay time constant (ring down time) can thus be written as:

$$\tau = \frac{l}{c(-\ln R + \alpha l)} \tag{2.22}$$

The ring down time, therefore, depends on the features of the cavity like the mirrors reflectivity, the cavity length and the absorbing species in the optical path.
In summary, a CRDS measurement consists of three steps: light injection inside the optical cavity, a rapid interruption of the light beam and an observation of the decay time. In the case of an empty cavity just the mirror's loss will be responsible for the exponential decay of the intensity. On the whole, better mirrors provide lower empty losses and higher sensitivity. It is obvious that the intensity of the light will take longer to decrease with mirrors of high reflectivity than with low reflectivity. As soon as an absorbing gas is present inside the optical resonator the exponential decay will be the result of a combination of the mirror losses and the absorption due to the gas inside the cavity. This then leads to a faster ring down, as shown in Figure 2.4.
The quantitative spectrum of the sample, obtained by subtracting the ring down rate of the empty cavity from the ring down rate of the cavity holding the sample, can be directly converted into the absorption coefficient:

$$\alpha = \frac{1}{c}\left(\frac{1}{\tau} - \frac{1}{\tau_0}\right) \tag{2.23}$$

The minimum absorption, which can be measured by CRDS, can be evaluated from the following equation:

$$\alpha_{\min} = \frac{1}{c}\left(\frac{1}{\tau_0 - \Delta t_{\min}} - \frac{1}{\tau_0}\right) \approx \frac{\Delta\tau_{min}}{c\tau_0^2} \tag{2.24}$$

Here $\Delta\tau_{\min}$ is the minimum measurable difference between τ an τ_0.

To improve the sensitivity of a CRDS measurement one can increase the ring down time by increasing the mirror reflectivity to make τ_0 maximum. The sensitivity limits of CRDS, its dynamic range and noise is well treated by Romanini and Lehmann [1993].

For the performance of absorption- measuring of an instrument the Noise-Equivalent Absorption (NEA) coefficient [van Zee et al., 1999] (NEA) is defined, being the minimum detectable absorption coefficient, which can be distinguished from empty cavity losses during a one second measurement interval with 1 sigma certainty, per square root of the data-acquisition rate (f_{rep}). We find:

$$NEA = \left(\frac{2}{f_{rep}}\right)^{1/2} \frac{\Delta\tau_{\min}}{c\tau_0^2} \tag{2.25}$$

Equation (2.25) indicates that increasing the acquisition rate or the ring down time and decreasing the $\Delta\tau_{\min}$, the NEA decreases. Moreover, the repletion rate needs to be large enough to estimate the standard deviation.

In the literature the NEA is defined also as 1σ root mean square noise level on the baseline of the spectra [Mazurenka et. al., 2005], and it has the dimension of cm^{-1} $Hz^{-1/2}$. By its definition, the NEA is species-independent. Typical NEA numbers for CRDS are in the range of $10^{-6} - 10^{-10}$ $cm^{-1}/\sqrt{Hz}$.

So far, we studied the behavior of the radiation inside the cavity, considering only the time domain. In a more rigorous way, we must consider same aspects of the intensity of the transmitted radiation in terms of frequency, which will allow us to introduce different parameters that will be encountered in the following chapters of this thesis.

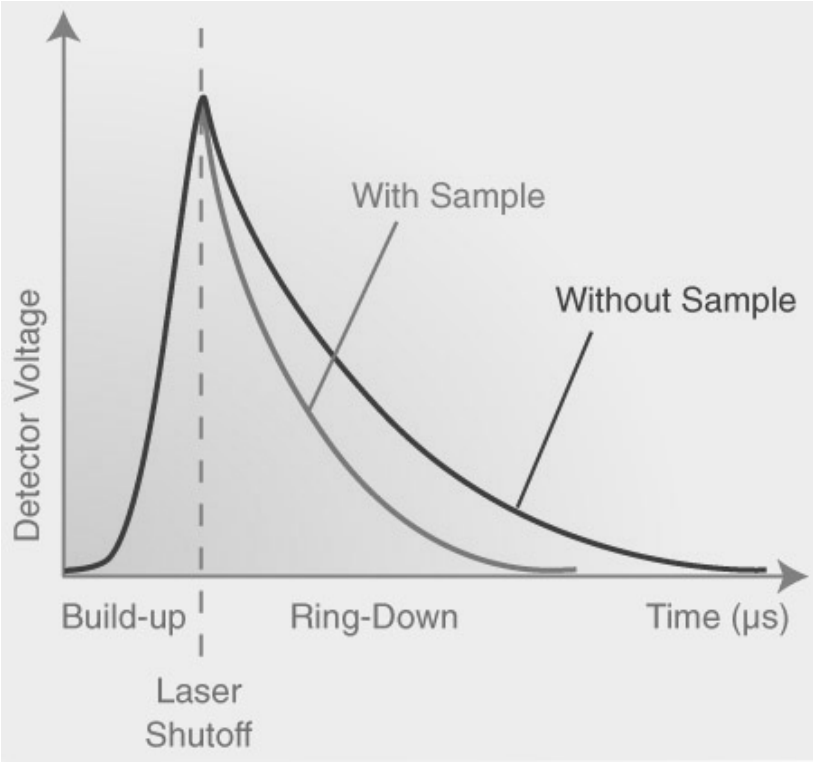

Figure 2.4: The laser signal, entering a cavity with and without sample, is shown as function of the time. The difference between the inverse decay rates is direct proportional to the sample concentration.

Considering the particular case in which the reflectivity coefficients R of the two mirrors are the same, the intensity of the transmitted radiation can be written [see, e.g., Demtröder, 2003]:

$$I(\nu) = I_0(\nu) \cdot \frac{(1-R)^2}{1+R^2-2R\cos\phi} \tag{2.26}$$

where ν is the input frequency of the radiation and ϕ represents the total phase difference between two successive beams inside the cavity and is equal to $\phi = \frac{4\mathrm{l}\pi\nu}{\mathrm{c}}$.

The transmittivity coefficient is now defined as the ratio between the incident initial intensity and the intensity of the transmitted beam [Demtröder, 2003]:

$$T = \frac{I_t(\nu)}{I_0(\nu)} = \frac{(1-R)^2}{(1-R)^2 + 4R\sin^2\left(\frac{2\pi l}{\lambda}\right)} \tag{2.27}$$

This function was first derived by G.B. Airy and determined for a Fabry-Perot interferometer. A Fabry-Perot interferometer is a multi-beam interferometer which, in its simplest form, comprises two parallel, optically flat, partially reflecting mirrors.

The total transmittivity is maximum when the denominator of Eq. (2.27) is minimum, that is, when the sine is zero. To be more precise:

$$\frac{2\pi}{c} l\nu = m\pi \tag{2.28}$$

Thus:

$$\nu_m = m\frac{c}{2l} = m\Delta\nu_l \tag{2.29}$$

The parameter $\Delta\nu_l = c/2l$ represents the frequency interval between two resonances and is called free spectral range (FSR), which depends on the distance l of the mirrors. The FSR is the ratio between the light speed and the round trip path length, since $2l$ is the round-trip path length The transmittivity depends on the frequency of the radiation and it is maximum only for one given frequency or one of its multiples. In other words, we observe that this optical system may be considered as a filter: with polychromatic input, only the frequencies, for which the transmittivity is maximum, can pass through.

The general behavior of the Airy function (Eq. 2.27) is shown in Figure 2.5. Curves are drawn for several values of the reflectivity. From this picture, we can see that the peaks become sharper as the mirrors reflectivity increases.

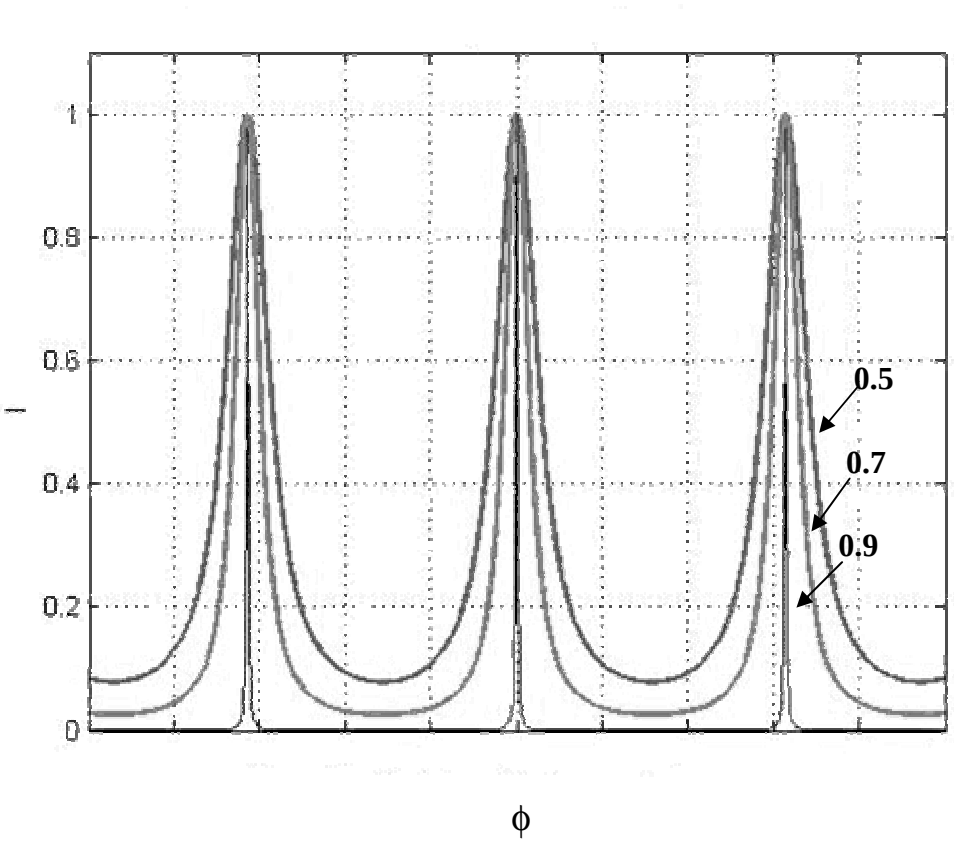

Figure 2.5: Transmission pattern showing the free spectral range (FSR) of a simple Fabry-Perot interferometer. Here are represented the cases in which R=0.5, R=0.7 and R=0.9.

The width of the cavity mode is given by the following equation:

$$\Delta\nu_c = \frac{c}{2\pi l}\frac{1-R}{\sqrt{R}} \tag{2.30}$$

We thus observe that the width of a cavity mode depends on the mirror reflectivity and on the cavity length *l*, whereas the free spectral range depends just on the cavity length.

Finally, the Finesse is defined as:

$$F = \frac{\Delta\nu_{FSR}}{\Delta\nu_c} = \frac{\pi\sqrt{R}}{1-R} \tag{2.31}$$

The finesse gives an indication of how separated and narrow the picks of the cavity are, or in other words, it measures the resolution of the interferometer. It is independent of the cavity length *l*.

A cavity can store energy only for the frequencies given by equation (2.29). The energy stored in an optical cavity is stored in what can be thought of as energy bundles. The energy bundles could pack parallel to the long axis of the resonator, which is known as the longitudinal or axial direction.
Another packing direction exists and it is perpendicular to the resonator axis. These are the transverse modes. Actually, the formal name is Transverse Electromagnetic Modes or TEM, to imply that the electric and magnetic field is on the whole perpendicular to the axial direction of the interferometer.
For every such transverse mode, there is a series of longitudinal modes, for which the round-trip phase shift is an integral multiple of 2π. Fox and Li [1961] calculated the most significant self-reproducing field configuration for a variety of mirrors.
The TEM are labelled with integral subscripts. The nomenclature and the general form of the TEM_{mn}. Modes characterized with m and $n > 0$ are the higher transverse mode, while mode with $m = n = 0$ are classified as fundamental modes.
The peculiarity of the latter is that they have an intensity distribution with a Gaussian profile. A complete dissertation of the propagation of Gaussian beam can be finding in several books, like the one of Siegman [1986] (ch. 16, pg. 630-648).

2.3.2 Various Implementations of CRDS

Whereas Fabry-Perot interferometers have been around for decades, the innovative idea of CRDS was the injection of a short laser pulse inside the optical resonator followed by the observation of the intensity decay. This method is usually denominated conventional CRDS. The first demonstration of a pulsed CRDS device is attributed to O'Keefe and Deacon [1988]. In their experiment, a pulsed dye laser, operating at a frequency of 690 nm, was used to detect CRD absorption spectrum of weak band of molecular oxygen.
In 1993, Lehmann and Romanini used ring down absorption spectroscopy to investigate vibrational overtones transitions of HCN and its isotopomers, $H^{13}CN$ and $HC^{15}N$.

Until 1997, CRDS experiments were performed applying pulsed lasers. In 1997, Romanini et al. demonstrated successfully a cavity ring down experiment with a continuous-wave (cw) laser, by using both a cw ring dye laser and an external cavity diode laser. In their experimental configuration, one cavity mirror was attached to a piezoelectric transducer in order to scan slowly the length of the cavity, in order to match the laser frequency to that of a longitudinal cavity mode, at least temporarily. They used two lenses and a spatial filter to make the input laser beam mode matched to the cavity TEM_{00} mode. After the photon intensity was built up in the cavity, the laser was interrupted with an acoustic-optic modulator and thus the decay signal could be detected.

Both pulsed and cw-CRDS have been used for isotope ratio determinations. In 2000, Dahnke et al. measured the isotopic composition of methane (^{12}CH4, $^{13}CH_4$) in natural air samples with a cw cavity ring down spectrometer, based on a CO overtone laser, operating in the wavelength region between 2.6 and 4.1 μm. They achieved a minimum detectable absorption of $1.9 \cdot 10^{-9}$/cm. Samura et al. [2001] determined the $^{18}O/^{16}O$ ratio of water vapor by using pulsed cavity ring down, with a Nd^{3+}:YAG pumped pulsed-dye laser, in the 960 nm-region. Finally, Wahl et al. [2006], performed measurements of carbon isotopes in carbon dioxide in 1.6 μm region. The CRDS system achieved a precision of 0.2‰.

The principle of cw-CRDS is now employed by two new commercial laser spectrometers, manufactured by Los Gatos Research [Los Gatos, 2008] and Picarro Inc [Picarro, 2008]. The laser spectrometer is applied for measurements of water both in liquid and vapor phase, and also for other species. The Picarro device uses a near-infrared DFB laser source that operates in the spectral region near 1.39 μm, and enters the sampling optical cell, which is composed by three high reflectivity mirrors (99.99%). A three-mirror cavity configuration is employed in order to support a continuous travelling light wave. This provides superior signal to noise ratio compared to a two-mirror cavity that supports a standing wave. A photodiode is employed in order to detect the light coming out from the output mirror and measure the ring down decay. The laser enters into resonance with the cavity by means of a piezoelectric actuator and in order to observe the different isotopologues of the water, the laser is firstly set to one wavelength λ_n and after that it is switched off to follow in

real time the ring down time and to convert it into absorbance. The same procedure is than repeated with the laser wavelength set to λ_{n+1} to scan the second isotopologue. The process is thus repeated according to the number of isotopologues to be investigated. Because of the fact that the laser is systematically tuned over the target absorption lines, the technique has been named Wavelength Scanned Cavity Ring Down Spectroscopy (WS-CRDS). The precision delivered by this instrument is of typically 0.5 ‰ for δ^2H and 0.1‰ for $\delta^{18}O$ in the case of the liquid water spectrometer, whereas for the water vapor instruments, the precision reached is 1‰ and 0.2‰ for δ^2H for $\delta^{18}O$, respectively. The lower precision in the latter case is not caused by the instrument itself, but rather by the introduction of the vapor sample into the cell.

The second company, Los Gatos Research, developed a commercial Liquid Water Isotope Analyzer and a Water-Vapor Isotope Analyzer, based on the OA- ICOS technique [Los Gatos, 2008]. They state for a water mixing ratio higher than 4000 ppm, a precision better than 0.2‰ and 1‰ with an integration time of 30 sec for the $^{18}O/^{16}O$ and $^2H/^1H$, respectively, and with a response time of 3 seconds. As OA-ICOS is not a CRDS technique in a strict sense, but rather a form of cavity enhanced absorption spectroscopy (CEAS), this technique will be further discussed in the following paragraph.

2.4 Technique of Cavity Enhanced Absorption Spectroscopy (CEAS)

2.4.1 Introduction

Cavity ring down spectroscopy, with a continuous-wave laser, can also be performed without temporal analysis of the ring down time. We have in this case a variant of the ring-down technique, called either Cavity Enhanced Absorption Spectroscopy (CEAS) or Integrated Cavity Output Spectroscopy (ICOS).

In CEAS, the laser light is coupled into the cavity and the intensity of the light leaking out of the cavity is detected. The key concept is that the frequency of the laser should be in resonance with one of the cavity modes. Instead of following the decay of the light in the cavity in real time, in a CEAS experiment, the temporal integration of the total transmitted intensity, which depends on the attenuation of the light trapped within the cavity by an absorbing sample, is measured. Since no fast detectors and

electronics are needed, this is the simplest cavity-based method and well-suited for a compact and robust portable analyzer.

Contrary to CRDS, CEAS does not require an acousto-optic modulator (AOM) or a mechanical chopping device to rapidly switch off the laser, in order to initiate a ring down event. However, the main challenge of this technique is to obtain the highest efficiency of injection of the laser into the cavity. This is because when the finesse of an optical cavity increases, the transmission mode envelope of the cavity becomes narrower, and this feature makes the injection of the light into the cavity more problematic.

In order to address this issue, a number of diverse implementations of CEAS were developed, among which we include:

1. Off-Axis Integrated Cavity Output (OA-ICOS)
2. Noise-Immune Cavity Enhanced Optical Heterodyne Spectroscopy (NICE-OHMS), and
3. Optical Feedback Cavity Enhanced Absorption Spectroscopy (OF-CEAS).

In OA-ICOS the alignment is similar to that of an astigmatic multipass Herriot cell [see, e.g. Herriott et al., 1964; McManus et al., 1995], with the exception that there is no entrance and exit hole in the mirror for the laser beam. The laser beam enters near one edge of a mirror and makes a long folded path. The distance between the mirrors and the radii of curvature determine the number of round trips, together with the chosen beam path.

The interaction between the laser and the cavity may be thought of as always resonant, eliminating the requirement of frequency locking by modulation of the cavity length. A very large number of TEM_{mn} modes are excited and they all contribute to the detection of the absorbing gas present in the cell and the technique is rather insensitive to vibrations. The main drawback of the OA-ICOS is the extremely reduced transmission through the cavity which demands the employment of a coherent radiation source with output power higher than 1 mW and very sensitive detectors [Paul et al. 2001; Maddaloni et al., 2006]. Another very significant drawback is that in this technique the large number of spots on the mirrors obliges larger mirrors, which means an increase of cavity volume and consequently an

increased gas exchange and/or a greater pumping requirement [Paldus and Kachanov, 2005]. Presumably, larger diameters mirrors help to increase the power stability in the cavity [J.B. Paul et al., 2001], and avoid interference given by the interactions of the rays within the cell.
OA-ICOS has been applied for detection of atmospheric trace gases and recently Engel et al. [2006] demonstrated an impressive sensitivity of $1.9 \cdot 10^{-12}$ $cm^{-1}/\sqrt{Hz}$. It is also the technique used in the commercial spectrometer of Los Gatos Inc. [Los Gatos, 2008].

One of the most sophisticated approaches, based on an actively locked cavity, is the so-called Noise-Immune Cavity Enhanced Optical Heterodyne Spectroscopy (NICE-OHMS) technique. This method is essentially a combination of the locking of the laser frequency to modes of the cavity and frequency modulation (FM) spectroscopy.
NICE-OHMS obtained the highest sensitivity reported for molecular spectroscopy applications corresponding to $1 \cdot 10^{-14}$ $cm^{-1}/\sqrt{Hz}$, for a saturated Lamb-Dip experiment [Ye et al., 1998]. In a "normal" absorption experiment, one order of magnitude less is expected. However, this technique is very complex because it depends on a careful matching between cavity length and modulation frequency, and because such high sensitivity demands extreme mechanical stability of the experimental setup.

The technique used in our project to measure water vapor isotopes in the higher troposphere and lower stratosphere is Optical Feedback Cavity Enhanced Absorption Spectroscopy (OF-CEAS) developed by researchers of the University of Grenoble, France [Morville et al., 2005]. In this method self-locking of the DFB laser frequency to the cavity mode is achieved thanks to the optical feedback (OF) from a V-shaped cavity.

The main advantage of this approach is that the self-locking very significantly improves the injection (and transmission) of the light into the high finesse cavity. A second benefit is that the spectrum is recorded only at the exact position of the cavity transmission and thus perfectly equidistant in frequency space. Finally, as opposed to OA-ICOS, the gas cell volume can be kept very small, enabling a fast instrument response with a modest flow rate.

In the following paragraphs a more detailed description of the OF-CEAS method is given.

2.4.2 Theoretical Description of OF-CEAS

In recent years, several semiconductor-laser frequency stabilization methods have been developed to respond to the urgent need of improvement of laser features like coherence, high spectral purity, side mode suppression, and linewidth narrowing. A number of these techniques are based on optical feedback. The phenomenon of the optical feedback was very well described by Laurent et al. [1989], by Ohshima and Schnatz [1991], and recently by Morville et al. [2005].

Optical feedback is introduced into a diode laser by returning some portion of the optical output back into the device. The prototypical example of a laser receiving optical feedback is a semiconductor laser receiving some of its own light back from a partially reflective plane mirror placed at a certain distance L from the laser. This is shown schematically in Figure 2.6.

The low coherence of a diode laser is a limiting factor in the efficient injection of high finesse optical cavities. The coherence may be increased, however, when the frequency selected optical field originating from a mode of a high finesse cavity is re-injected into the diode laser.

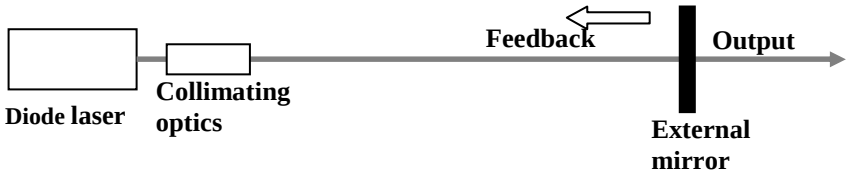

Figure 2.6: Schematic overview showing diode laser subject to optical feedback.

2.4.3 Feedback and V-shaped Cavity

A modification of the experimental setup based on the Fabry-Perot principle of Figure 2.6 is depicted in Figure 2.7. In this case, the diode laser beam is coupled into the V-shaped high finesse ($F>10^4$) cavity, made by three high reflectivity mirrors, *M1*, *M2* and *M3*, with a radius of curvature of 1 m. The length of the folded cavity is about 0.5 m. Two photodiodes are used, one to reveal the reference signal, another to detect the cavity transmission. This V-shaped optical geometry prohibits the direct reflection

from input mirror *M1* to arrive back to the laser, to avoid unwanted instabilities in the laser output. On the other hand, part of the radiation, which is build up in the cavity does come back to the diode laser.

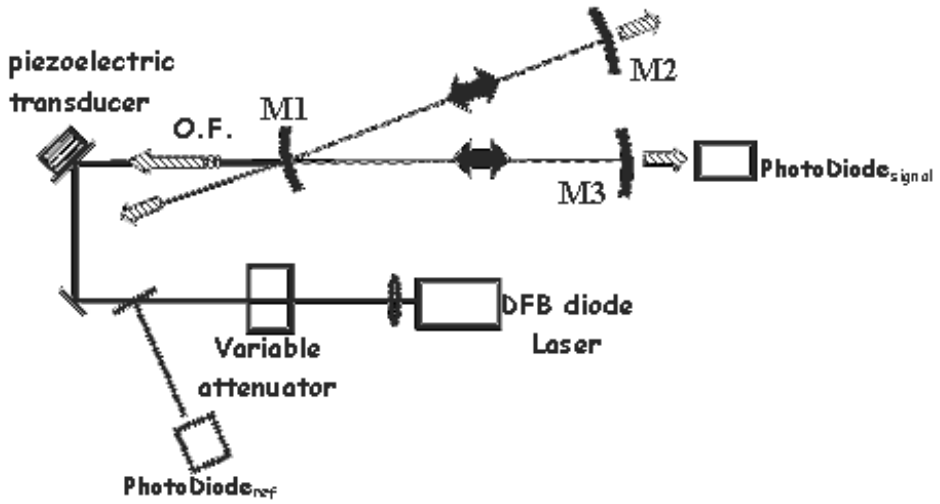

Figure 2.7: Scheme of the experimental setup: Piezoelectric Transducer: Piezo transducer - mounted mirror, M1, M2, M3: High reflectivity mirrors; $PhotoDiode_{ref}$: reference photodiode, $PhotoDiode_{signal}$: cavity transmission signal photodiode.

When the resonant light, which has spent some time inside the cavity, is sent back to the diode laser, the cavity assumes the role of an extension of the optical feedback region of the laser itself with much better sensitivity. Figure 2.8 explains this phenomenon.

A periodic ramp is applied to the diode laser current and the laser locks and relocks to the successive cavity modes. If the laser frequency is far from matching a cavity resonance (also referred to as a mode in the following), the level of optical feedback is extremely low and the laser frequency tunes according to the changes in the injection current. As the laser frequency is approaching a cavity mode, optical feedback builds up and the laser frequency locks to the cavity mode, even when the laser current continues to scan. The optical locking of the laser frequency to the reference cavity resonance is observed directly with a photodiode, which detects the power transmitted through the cavity as a function of the laser current. The main feature of this transmission function is that of a flat top.

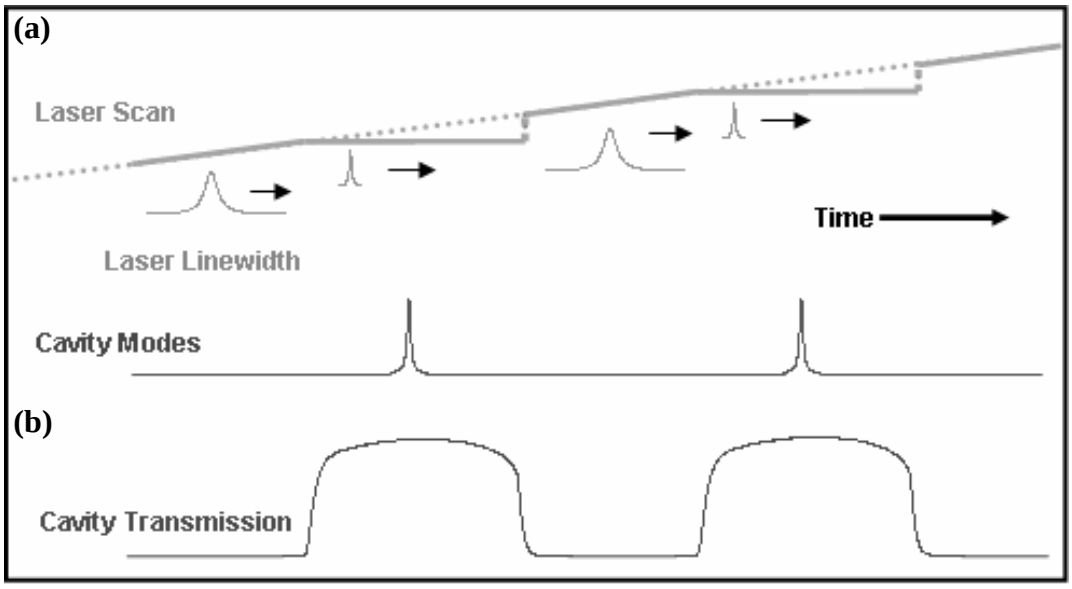

Figure 2.8: Principle of laser – cavity resonance in the OF-CEAS. a) Optical feedback produces a strong effect, which narrows the laser emission spectrum and the frequency of the laser is temporary in resonance with a mode of the cavity. b) Cavity transmission signal.

This abrupt flattening in the scan indicates that the laser frequency is stabilized to the frequency of a peak transmission of the cavity resonance. At the end of the locking range the laser drops out of lock and continues to scan, as can be seen in Figure 2.8. The frequency range over which the diode laser locks depends on the amount of returned power and the phase of the feedback, as well as on characteristics of the diode laser. The amount of feedback is adjusted using a rotatable half-wave plate and a linear polarizer, in such a manner that the laser frequency remains in resonance with each cavity mode long enough to reach maximum injection efficiency, without ever missing a mode when hopping from one to the next neighboring mode.

It has, therefore, the added advantage that the cavity longitudinal mode structure is used to probe the absorption spectrum at frequencies equally spaced by the cavity free spectral range. There is thus essentially no noise on the frequency scale of the absorption spectra, facilitating a precise fit of the spectral features.

As we will see in Chapter 3 and 5, the cavity used in our spectrometer is made of thick stainless steel, and mirrors are glued on the cavity with no adjustment

mechanism interposed. Moreover, each OF-CEAS spectrum is obtained during a 200ms laser scan. Because of that, on this time scale and given the cavity stiffness changes in cavity length are negligibly small.

The optical lock generally requires a low level of feedback: the optical feedback is of the order of 10^{-4} of the laser output power. Besides the laser frequency being locked to a cavity mode, the laser line width also narrows to below the width of the cavity resonance, which is typically three orders of magnitude narrower than the (long-term) free-running laser line width.
In order to have the optimum coupling of the cavity to the diode laser, not only the amount of radiation – the feedback ratio – that returns to the laser needs to be controlled, but also its optical phase. The phase of the light re-injected into the laser is responsible for the profile of the cavity transmission signal and for the maximum optical feedback. The optical phase depends on the laser – cavity distance. The condition to have the right optical phase is that the path-length between the laser diode and the cavity be equal to an integral number of the cavity length.

Coarse adjustment of this path-length can be done simply by translating the diode laser mounting. Once this is adjusted, a folding mirror, mounted on a piezoelectric transducer (PZT), provides a means for fine-adjustment of the laser-to-cavity distance, and thus for controlling the phase of the optical feedback to the laser. The control is performed by a relatively slow (80 Hz bandwidth), analogue electronic feedback loop that uses an error signal derived from the symmetry of the cavity transmission modes.
In case the shape of the mode is symmetric, no correction is applied to the piezo and thereby the integrated signal is zero. If the shape of the modes is asymmetric, corresponding to an improper phase condition, the integrated signal drives the piezo in the correct direction.

Figure 2.9 gives a final overview of the main signals of the OF-CEAS spectrometer. The raw cavity transmission signal, together with the current ramp is shown. The same picture also shows the data acquisition (daq) trigger and the laser-off signals. The daq trigger determines when the computer has to start the spectrum acquisition. At predetermined positions in the scan (or even once in a number of scans), the laser-

off signal triggers the laser current to go to zero for a duration of 150 μs, exactly when the laser passes through resonance with a cavity mode. At this point a ring down event is recorded.
The ring down allows the calibration of the absorption scale of the CEAS spectra. The ring down time of the spectrometer is just over 20 μs, corresponding to an effective absorption path length of 6 km. The laser-off signal is also used to trigger a zero-reading of the photodiode, in order to correct for possible detector bias drift.
The conversion of the spectra to absolute absorption units is made using the ring down time determined for one pre-selected mode in the spectrum as described above. The mathematical approach is explained in more detail in chapter 3. Ring down events are recorded at a rate of 1 MHz for a total time approximately 10 times longer than a typical ring down time of 20 μs. For this measurement, the laser is abruptly turned off, at the top of the cavity transmission, enabling the subsequent ring down event to be recorded by the signal photodetector.

In conclusion, the OF-CEAS technique of optically locking the laser frequency to a cavity mode presents an elegant solution to the problem of injecting a sufficiently large amount of laser light into a spectrally very narrow cavity mode, a problem encountered in all implementations of CEAS techniques.

In the next chapter, a detailed description of the instrument design, the data analysis procedure and first instrument performances both in laboratory and aircraft platform will be reported.

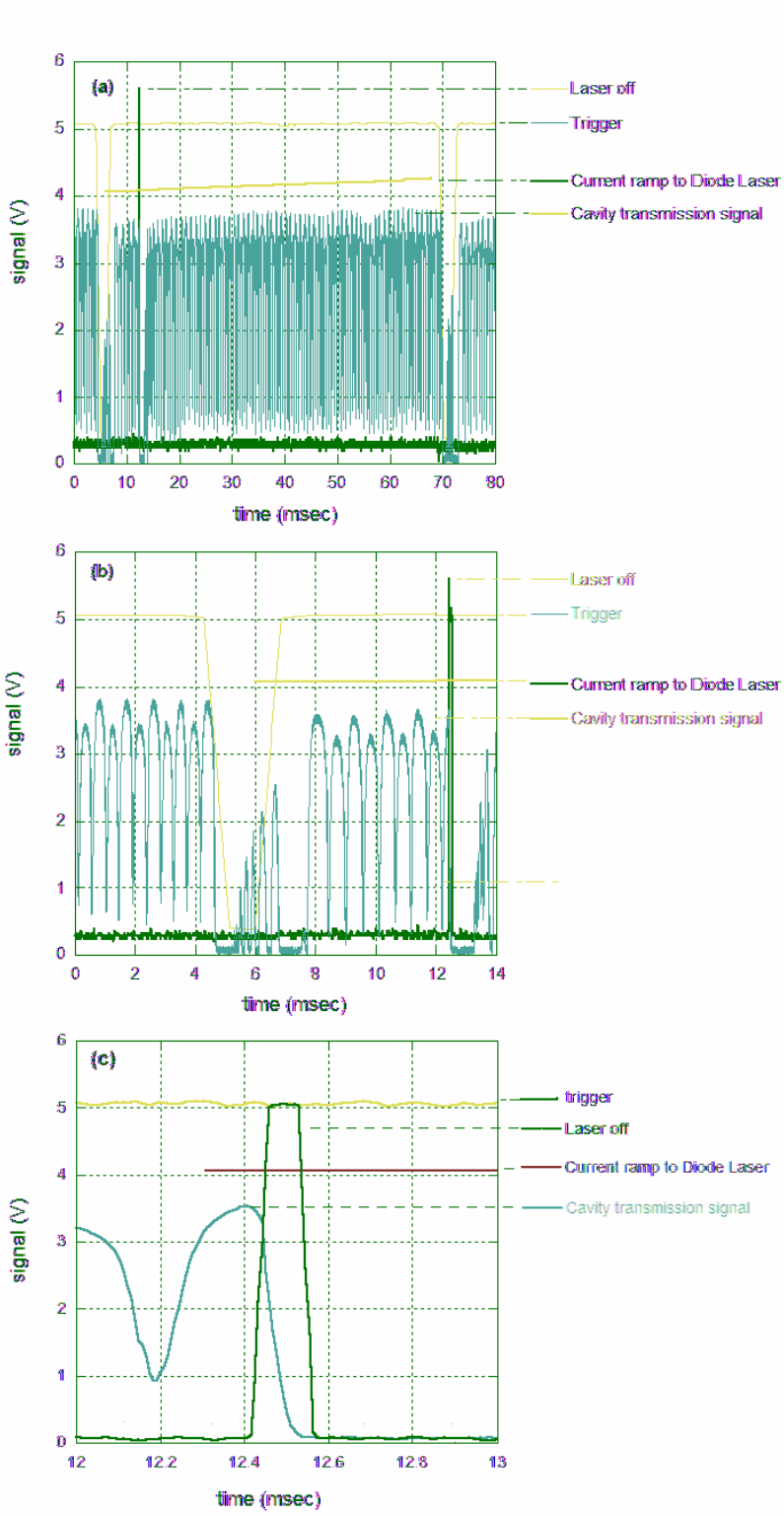

Figure 2.9: (a) Main Signals of the OFCEAS: Trigger, Ramp, Cavity transmission and laser off; (b) and (c) Detail of the previous figure on an expanded horizontal scale. The laser off and the trigger have been sampled using a digital oscilloscope.